Remote Sensing for Environmental Monitoring and Change Detection (Proceedings of Symposium HS3007 at IUGG2007, Perugia, July 2007). IAHS Publ. 316, 2007.

Evaluating actual evapotranspiration by means of multi-platform remote sensing data: a case study in Sicily

MARIO MINACAPILLI[1], GIUSEPPE CIRAOLO[2], GUIDO D'URSO[3] & CARMELO CAMMALLERI[2]

1 *Dept of Engineering and Agro-Forestal Technology (ITAF), Università di Palermo, Viale delle Scienze I-90128, Palermo, Italy*
minacap@idra.unipa.it

2 *Dept of Hydraulic Engineering and Environmental Applications, Università di Palermo, Viale delle Scienze I-90128, Palermo, Italy*

3 *Dept of Agricultural Engineering and Agronomy University of Naples "Federico II", Italy*

Abstract During the last two decades, the scientific community developed detailed mathematical models for simulating land surface energy fluxes and crop evapotranspiration rates by means of an energy balance approach. These models can be applied in large areas and with a spatial distributed approach using surface brightness temperature and some ancillary data retrieved from satellite/airborne remote sensed imagery. In this paper a district scale application, in combination with multispectral satellite and airborne data has been carried out to test the potential of two different energy balance models to estimate evapotranspiration fluxes from a set of typical Mediterranean crops (wine, olive, citrus). The impact of different spatial resolutions on model-derived fluxes has been investigated in order to understand the roles and the main conceptual differences between the two models which use a "single-layer" (SEBAL) and a "two-layer"(TSEB) schematization, respectively. The critical spatial resolution of remote sensed data has been also investigated.

Key words actual evapotranspiration; spatial resolution; surface energy balance

INTRODUCTION

A correct estimation of temporal and spatial distribution of evapotranspiration (*ET*) is an essential step for water management and crop water requirements, in particular in Mediterranean areas where water scarcity and semiarid climate often cause fragility and severe damage in the agro-ecosystems. The determination of *ET* is not simple, due to the heterogeneity and complexity of hydrological processes. Following these needs, recently, the scientific community developed detailed mathematical models for simulating land surface fluxes by means of an integrated use of ancillary data and remote sensing observations to gather quantitative information on the temporal and spatial distributions of many surface soil and canopy parameters (Menenti, 2000). Many algorithms to estimate surface energy fluxes and evapotranspiration based on remote sensed imagery have been proposed. Some reviews can be found in Kustas & Norman (1996), Chehbouni *et al*. (1997), Bastiaanssen (1998) and Schmugge *et al*. (2002).

A common way to estimate *ET* is to rearrange the energy balance equation for the land surface, solving for the latent heat flux, λET (W m^{-2}), as a residual term:

$$\lambda ET = R_n - G_0 - H \quad (1)$$

where R_n (W m^{-2}) is the net incident radiation, G_0 (W m^{-2}) is the soil heat flux, and H (W m^{-2}) is the sensible heat flux, the heat exchange between surface and atmosphere because of the temperature gradient. Typically, with reliable estimates of solar radiation, differences between remote sensing estimates and observed $R_n - G_0$ are within 10%. The largest uncertainty in estimating λET comes from computing H. Following a classical approach of micrometeorology (Brutsaert, 1982) the sensible heat flux H of the atmospheric boundary layer close to the surface (where energy exchange occurs because the potential temperature gradient) can be expressed by the:

$$H = \frac{\rho c_p \Delta T}{R} = \frac{\rho c_p (T_{oh} - T_A)}{R} \quad (2)$$

where ρ (Kg m^{-3}) is the air density, c_p is the specific heat of air (J Kg^{-1} K^{-1}), T_{oh} is the so-called "aerodynamic surface temperature", T_A is the air temperature at some reference height above the canopy, and R is the total resistance to heat transfer between the nominal source height corresponding to T_{oh} and to the reference height. If radiometric temperature, T_r, is used as aerodynamic surface temperature, then an additional resistance, called "excess resistance", has to be computed in order to take into account the non equivalence of T_{oh} and T_r. To this aim, various approaches have been proposed over the years to solve this problem (Norman *et al.*, 1995; Bastiaanssen *et al*., 1998a,b).

For a homogeneous land cover a "*single source*" approach can be applied. In this way an empirical adjustment of R is performed, assuming a linear relationship between T_r and $\Delta T = (T_{oh} - T_A)$ to be calibrated on the basis of the knowledge of two boundary conditions (a dry non evaporating land unit and a fully wet surface). This approach treats the unique soil-canopy layer as semi-transparent for the radiation input. It works well only under limited surface conditions, but not in the cases where radiometric temperature depends on the vegetation/soil interactions within the unit area.

On the other hand a *"two sources*", consisting of vegetation and soil layers, takes into account this heterogeneity and can explicitly accommodate the major factors that influence radiometric and aerodynamic temperatures. This approach uses two sets of soil and canopy aerodynamic resistance, connected in series or parallel to take into account the interaction between vegetation and soil energy fluxes components.

In this paper the SEBAL single source model (Bastiaanssen *et al*., 1998a,b) and the TSEB two source model (Norman *et al*., 1995) have been applied to simulate the surface energy fluxes in an agricultural area located in Sicily: this study area is characterized by typical crops-field, whose dimensions usually require a high spatial resolution data set. In order to assess the pixel-size influence we used both satellite and airborne imagery data sets. The comparison between airborne and satellite application allowed the identification of the critical spatial resolution to correctly simulate the energy fluxes in the study area.

MODEL DESCRIPTION

A detailed description of SEBAL and TSEB models can be found in Norman *et al*. (1995); Bastiaanssen *et al*. (1998a,b); Kustas & Norman (1999a,b). A first application

of the models in the same study area can be found in Ciraolo *et al*. (2006). Here we only describe the main differences of the models, with particular attention on the sensible heat flux, *H*, computation.

In both models the total net radiation estimation R_n, can be performed, computing the net available energy by taking into account the rate lost by surface reflection in the shortwave (0.3 / 2.5 μm) and emitted in the longwave (6/100 μm):

$$R_n = (1-\alpha)R_{swd} + \varepsilon_0\left(\varepsilon'\sigma T_a^4 - \sigma T_0^4\right) \tag{3}$$

where R_{swd} is the global incoming solar radiation in the short wave, α is the surface albedo, ε′ is the atmospheric emissivity, ε_0 is the surface emissivity (–), σ (W m^{-2} K^{-4}) is the Stefan-Boltzmann constant, T_a (K) is the air temperature, while T_0 (K) is the land surface temperature derivable from thermal remote sensing data.

Moreover, the TSEB model splits the net radiation R_n between the canopy ($R_{n,C}$) and soil ($R_{n,S}$) is explicitly computed as a function of Leaf Area Index, *LAI*:

$$R_{n,S} = R_n \exp\left(-0.45LAI/\sqrt{2\cos(\theta_z)}\right) \tag{4}$$

$$R_{n,C} = R_n - R_{n,S} \tag{5}$$

where R_n is computed using again equation (3) and θ_z is the solar zenith angle.

The soil heat flux, G_0 (W m^{-2}), is computed using the empirical approach: in SEBAL the G_0 is expressed as a semi-empirical fraction of R_n, taking into consideration the albedo α, the *NDVI* vegetation index, and the surface temperature T_0:

$$G_0 = R_n \frac{T_0}{\alpha}\left(0.003\alpha + 0.006\alpha^2\right)\times\left(1 - 0.98NDVI^4\right) \tag{6}$$

Differently in the TSEB, the soil heat flux G_0 is expressed as a fraction c_g (≈ 0.35) of the net radiation at the soil surface $R_{n,S}$.

The estimation of sensible heat flux *H* solving equation (2) requires the computation of the aerodynamic resistance, *R*, which in SEBAL on the basis of the single layer approach is given by:

$$R = \frac{\left[\ln\left(\frac{z-d_0}{z_{0,M}}\right) - \psi_M\left(z, L_{MO}\right)\right]\cdot\left[\ln\left(\frac{z-d_0}{z_{0,H}}\right) - \psi_H\left(z, L_{MO}\right)\right]}{k^2 \cdot u} \tag{7}$$

where *k* (-) is the von Karman's number, *u* (m s^{-1}) is the wind speed at height z, Ψ_H (-) and Ψ_M (-) are two stability correction functions for momentum and heat transfer, respectively, and L_{MO} is the Monin-Obhukov length (-). Both correction functions Ψ_H, Ψ_M, and Monin-Obhukov length L_{MO} depends on *H* and then on *R*. For this reason the solution of equations (2) and (7) is calculated by means of an iterative method. Furthermore, as stressed in the previous paragraph, in SEBAL the empirical adjustment of the resistance term due to the use of radiometric temperature instead of the surface temperature, is taken into account, assuming a linear relationship between T_r and $\Delta T = (T_{oh} - T_A)$ to be calibrated on the basis of the knowledge of two boundary conditions (a dry non evaporating land unit and a fully wet surface).

Differently the TSEB scheme considers the contributions from the soil and the canopy separately and uses a few additional parameters to solve for sensible heat. In

particular the sensible heat flux, H, is expressed as the sum of the contribution of the soil, H_s, and of the canopy, H_c, according to the assumption of parallel resistance network arrangement. This allows rearranging the resistance term in equation (2) by using the following expression:

$$\overline{R} = \frac{T_r - T_A}{\left[\frac{T_C - T_A}{R}\right] + \left[\frac{T_S - T_A}{R + R_S}\right]} \tag{8}$$

where T_C is the canopy temperature, T_S is the soil temperature and R_S is the soil resistance to the heat transfer.

An estimate of vegetation directional fractional cover f_θ is used to estimate T_C and T_S form T_r using the following equation:

$$T_r = \left[f_\theta T_C^4 + (1 - f_\theta) T_S^4\right]^{1/4} \tag{9}$$

while R_S is computed from a relatively simple formulation predicting wind speed near the soil surface (Goudriaan, 1977; Norman *et al*., 1995; Kustas & Norman 1999a,b).

With the additional use of the Priestley-Taylor formulation (Priestley & Taylor, 1972) for estimating canopy transpiration and consequently T_C, then the closure of the set of available equations (equations (8) and (9)) is achieved. Since the Priestly-Taylor formulation is appropriate for well-watered grass surfaces in the TSEB model the use of a greenness factor, f_g, to account the specific crop conditions, has been proposed. If no information is available on f_g the authors suggest it should be set to unity (Norman *et al*., 1995).

For both models, once the R_n, G_0 and H spatial distributions are obtained, the instantaneous λET (W m^{-2}) spatial distribution is computed using equation (1). The daily integration of λET and the computation of the ET_d (mm d^{-1}), can be performed using the evaporative fraction parameter, Λ (Menenti & Choudhury, 1993):

$$\Lambda = \frac{\lambda ET}{R_n - G_0} \tag{10}$$

Several studies (Brutsaert & Sugita, 1992; Crago, 1996) demonstrate that, within daytime hours, the Λ (0–1) values are almost constant in time. This fact suggests using the Λ parameter as a temporal integration parameter. Following this consideration, the ET_d spatial distribution can be derived using the:

$$ET_d \cong \Lambda \frac{R_{n,24}}{\lambda} \tag{11}$$

where λ (MJ Kg^{-1}) is the latent heat of vaporization and $R_{n,24}$ represents the averaged net daily radiation that can be derived by direct measurement or classical formulation proposed by FAO publications (Allen *et al*., 1998).

Case study and DATA DESCRIPTION

The above mentioned approaches were applied in a test area covering approximately 255 ha within the irrigation district “Basso Belice” (Fig. 1), located in the western

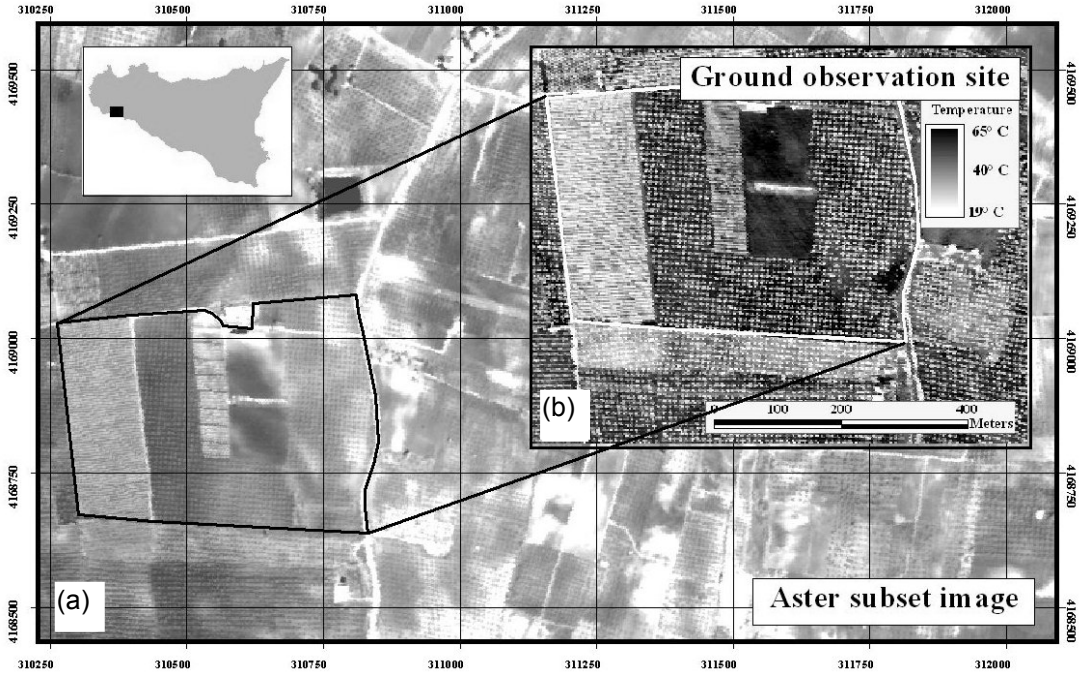

Fig. 1 (a) Geographic location of the study area and (b) subset test area from airborne data-set (surface temperatures derived from ATM sensor).

coast of Sicily, in which land use is predominantly for arboreal crops (mainly olives, grapes and citrus fruits). The study area is mainly characterized by a typically Mediterranean climate: during 2005 the total annual rainfall was about 700 mm, with an annual reference evapotranspiration of about 1100 mm. The soils are mainly alluvial deposits characterized by loam and sandy loam textures.

Two different imagery data sets were acquired during spring and summer 2005: one airborne NERC (Natural Environmental Research Council) data set, acquired in May, including an ATM (Airborne Thematic Mapper) image and a CASI-2 (Compact Airborne Spectrographic Imager) image, both characterized by high spectral and spatial resolution (3 m) and an ASTER satellite image, acquired in August, characterized by a 15-m spatial resolution in three visible-near infrared bands and 90-m resolution in five thermal infrared bands.

Inside the study area a smaller subset (Fig. 1(b)) has been used as ground observation site, where standard agro-meteorological data, scintillometer (Scintec SLS20 model) based flux components and spectroradiometer measurements have been collected during aircraft and satellite overpasses.

Remote sensing data pre-processing

The NERC airborne overflight was performed on 16 May 2005 at about noon (local time). The study area was acquired from a distance of 1400 m in three flight tracks. The nominal spatial resolution is 2.5 m.

From the radiometric point of view the ATM sensor records the incoming radiation in 11 spectral bands ranging from visible and near-infrared (VIS/NIR, bands

1–8), short-wave infrared (SWIR, band 9 and 10) to the thermal infrared (TIR, band 11). The CASI-2 sensor has been setup to record the spectral radiance in visible and near-infrared bands using a multispectral acquisition that uses 12 bands precisely placed narrow wavelengths to measure specific vegetation phenomena.

At the same time of the image acquisition a field survey was carried out by measuring spectral and vegetation parameters in correspondence of predefined targets: in order to perform the radiometric correction of the images, several spectral measurements have been also acquired on homogeneous targets (asphalt, sand, bare soil, vegetation) by using an ASDI FieldSpect HH spectroradiometer. For the scope of the present study we used all the bands acquired by the CASI-2 sensor and the thermal infrared band of ATM sensor to map the surface temperature. An empirical line method (Slater *et al*., 1996) was applied to calibrate CASI-2 bands in reflectance and to correct the atmospheric influence: albedo and vegetation index distributions were calculated using these corrected bands.

The temperatures recorded by the ATM thermal band were compared with the ground temperatures measured at several points at the same time of the acquisition and an empirical adjustment has been applied. Figure 2(a) and (b) shows the accuracy obtained from the abovementioned corrections in both CASI-2 VIS/NIR spectral range and ATM thermal band.

The geometric correction of the entire data set has been performed using the NERC Azgcorr software that performs geocorrection of ATM and CASI-2 data using aircraft navigation data and Digital Elevation Model (DEM) of the acquired zone.

The ASTER image of the study area was recorded on 16 August 2005 at about 11:00 h (local time). The image data has been geometrically and radiometrically calibrated (Epema, 1990) and atmospherically corrected (Chavez, 1988). As regards the thermal bands, the atmospherically corrected radiometric temperature has been retrieved using field temperature measurements acquired at the same moment of the satellite overpass.

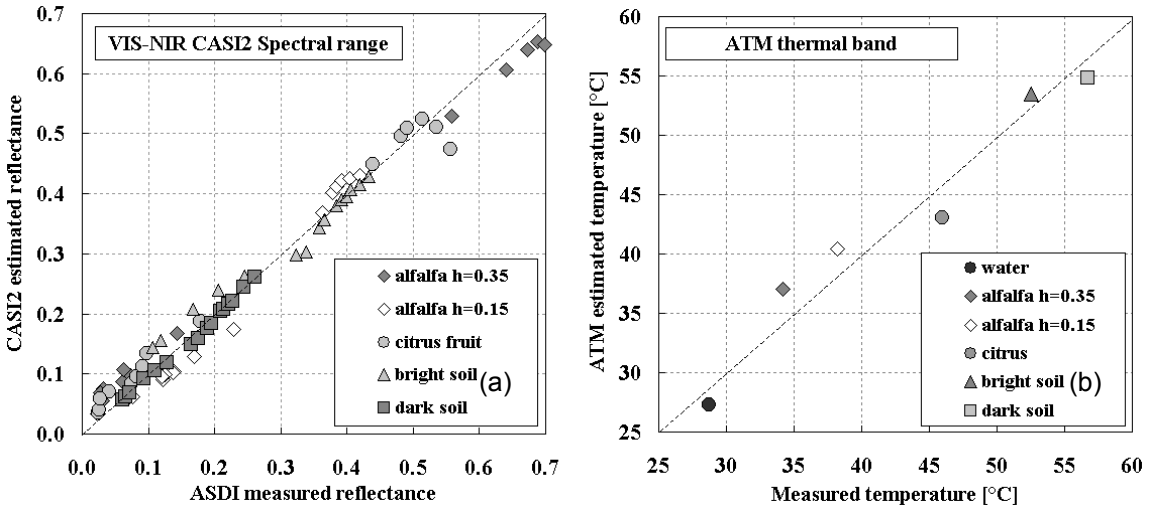

Fig. 2 Validation of correction procedures used to calibrate VIS-NIR CASI2 and ATM thermal bands.

RESULTS

SEBAL and TSEB models have been applied using the two sets of data retrieved from the remotely sensed airborne and satellite images described in the previous paragraphs as input. The outputs of the models have been analysed and compared either in terms of spatial distribution, or in terms of pixel-by-pixel scatterplots.

The pixel size effect has been analysed not only by the comparison of the results of simulations using the NERC and ASTER data set, but also degrading the resolution of the NERC airborne imagery (3 × 3 m) to the resolution of the ASTER satellite image (90 × 90 m).

SEBAL *vs* TSEB: NERC data

Figure 3(a),(b) show the daily evapotranspiration (ET_d) spatial distribution obtained by applying the SEBAL and TSEB models on the airborne data. The comparison of the two spatial distributions doesn't display a significant difference, showing similar patterns of evapotranspiration values.

Scatterplots reported in Fig. 4(a)–(c) show the comparison of each flux as simulated by the two models: some difference can be found in this graphs. The ET_d assessment, as evidenced in the spatial distribution analysis, are very similar (Fig. 4(c)), but this is due to a compensation effect in the G_0 and H estimations.

In fact, the G_0 distribution obtained by the SEBAL model are overestimated compared to the TSEB ones (Fig. 4(a)): in particular differences of 20–30 W m^{-2} can be found in zones characterized by low LAI values ($0 < LAI < 1$).

Moreover the G_0 values calculated by SEBAL show a low variability around the value of about near 110 W m^{-2}, while TSEB estimations vary within the 80–140 W m^{-2} range. This overestimation is compensated for by the under-estimation of the sensible

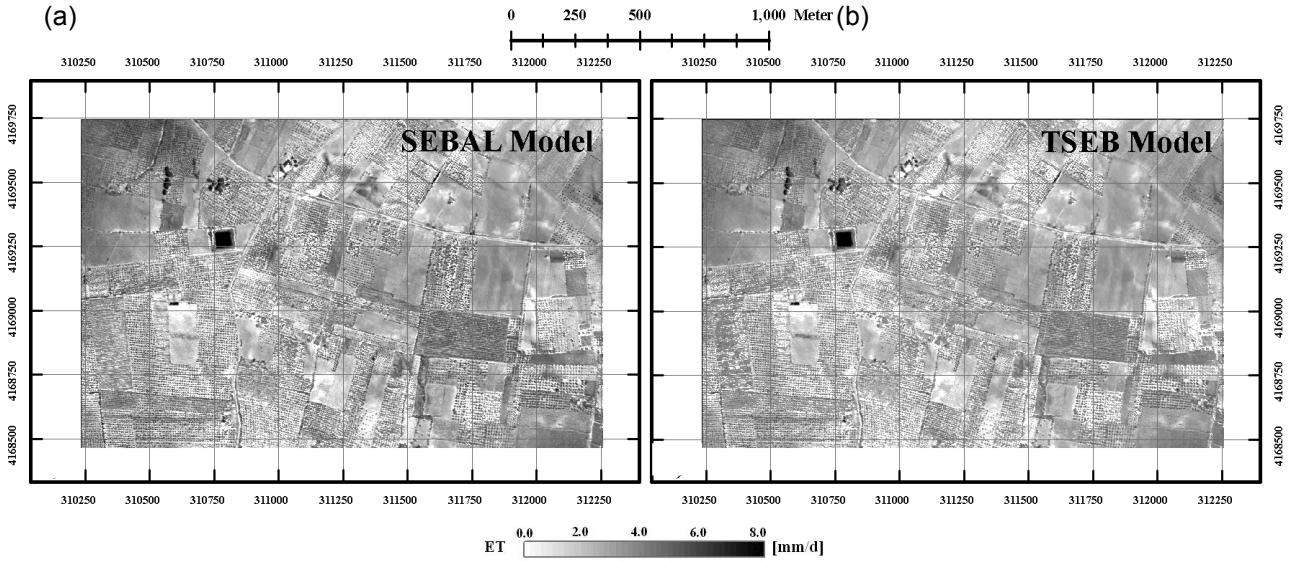

Fig. 3 Daily ET maps obtained from NERC airborne imagery using (a) SEBAL and (b) TSEB models.

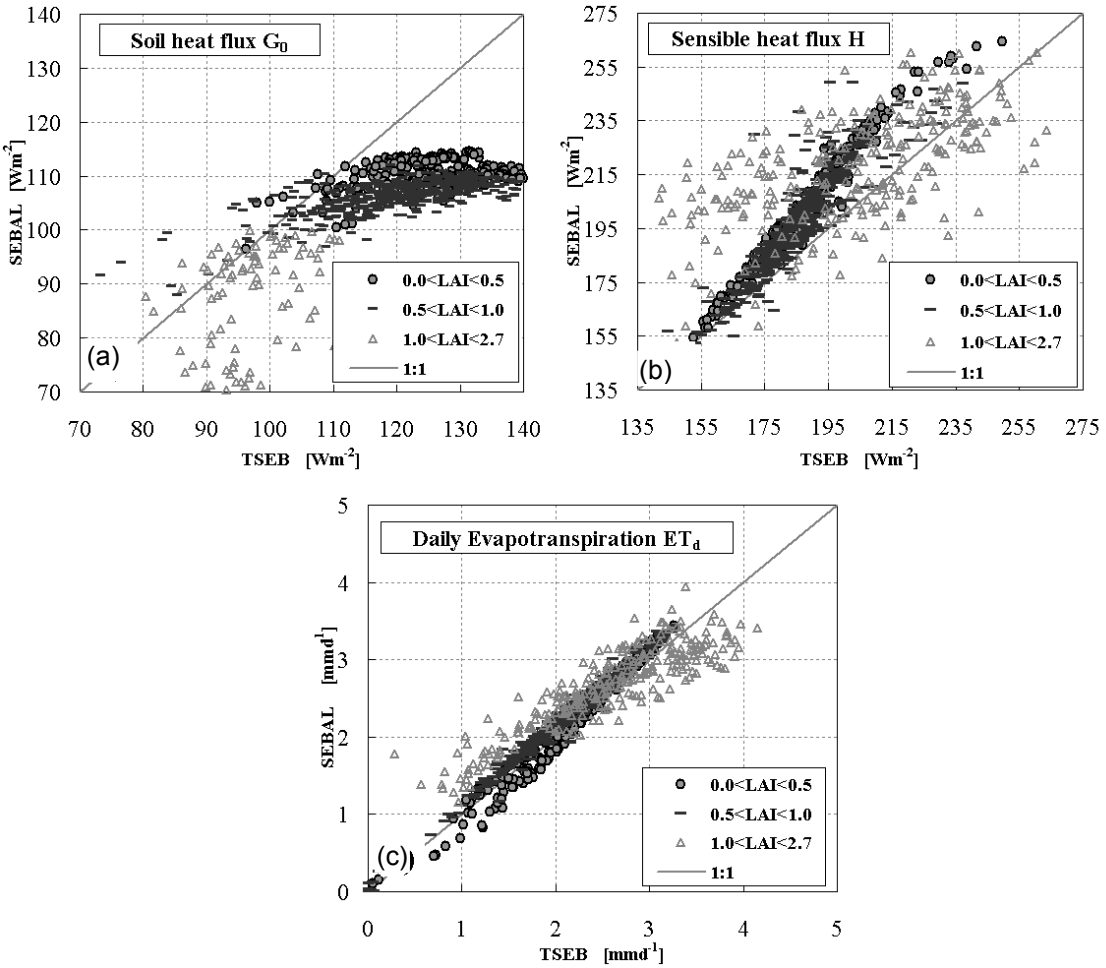

Fig. 4 Scatterplots of SEBAL *vs* TSEB modelled fluxes and evapotranspiration outputs derived using NERC data set.

heat H values calculated by SEBAL compared with the TSEBS ones (Fig. 4(b)). The abovementioned underestimation, already reported in the literature (Ciraolo *et al*., 2006), has been found in each vegetation class, with a range of variability between 20 and 60 W m^{-2}.

The overestimation of instantaneous sensible fluxes, H, which also results in similar studies (Savige *et al*., 2005; Ciraolo *et al*., 2006), can be related to an underestimation of the aerodynamic resistance to the heat transport, since SEBAL does not take into account the soil–canopy interactions.

The abovementioned behaviour has been partially confirmed by the ground truth data collected during the airborne overpass: energy fluxes were acquired using a scintillometer (Scintec SLS20 model) and other micrometeorology sensors located over an alfalfa field (0.5 ha in area) well defined in the high resolution images. Table 1 shows the comparison between measured and modelled values. R_n estimates are within 12 W m^{-2} from measured values, while the most significant differences were observed in G_0 and H simulated values. In these cases, both SEBAL and TSEB estimations exceed the measurements, causing an underprediction of ET_d. However, the observed differences can be considered acceptable for TSEB estimations, causing an

Table 1 Comparison between scintillometer based measurements and model flux estimates. In parentheses are reported the standard deviation of measured and modelled values.

Average flux		Measured	SEBAL	TSEB
R_n	(W m^{-2})	431 (33)		419 (17)
$R_{n,s}$	(W m^{-2})			184 (36)
$R_{n,c}$	(W m^{-2})			235 (32)
H	(W m^{-2})	83 (16)	146 (28)	105 (13)
H_s	(W m^{-2})			43 (9)
H_c	(W m^{-2})			61 (8)
G	(W m^{-2})	49 (6)	58.7 (10)	65 (13)
ET_d	(mm d^{-1})	4.5	3.5 (0.6)	4.1 (0.3)

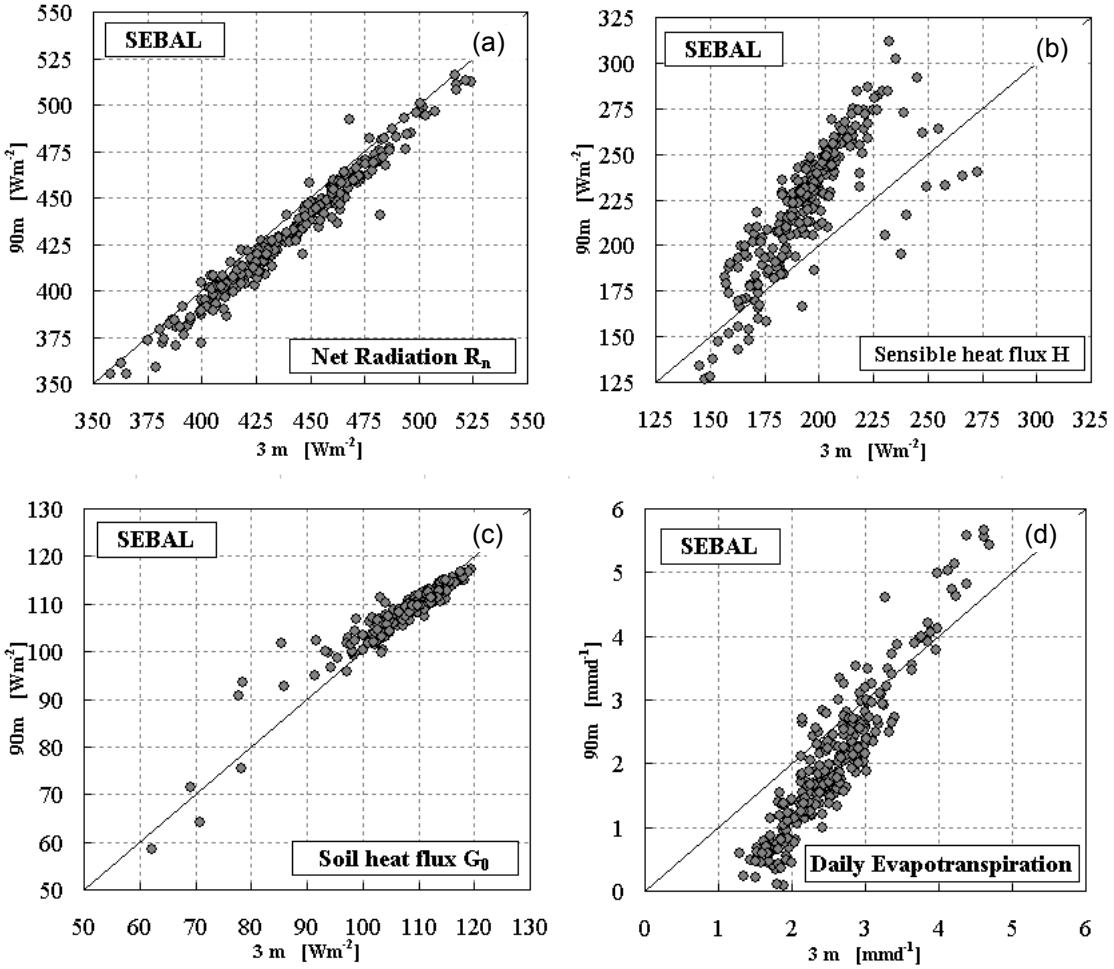

Fig. 5 Scatterplots of 3-m *vs* 90-m model outputs obtained using SEBAL.

underestimate of λET of about 33 W m^{-2}, while in SEBAL this underestimate is about 74 W m^{-2}, producing an underestimation of ET_d of about 1 mm d^{-1}.

Figures 5(a)–(d) and 6(a)–(d) show the pixel size effect on the energy fluxes resulting from the SEBAL and TSEB models. In this first analysis, the airborne data images were degraded in order to obtain a 90-m resolution similar to the ASTER thermal bands. In this case the SEBAL model overestimates H, compared to the value

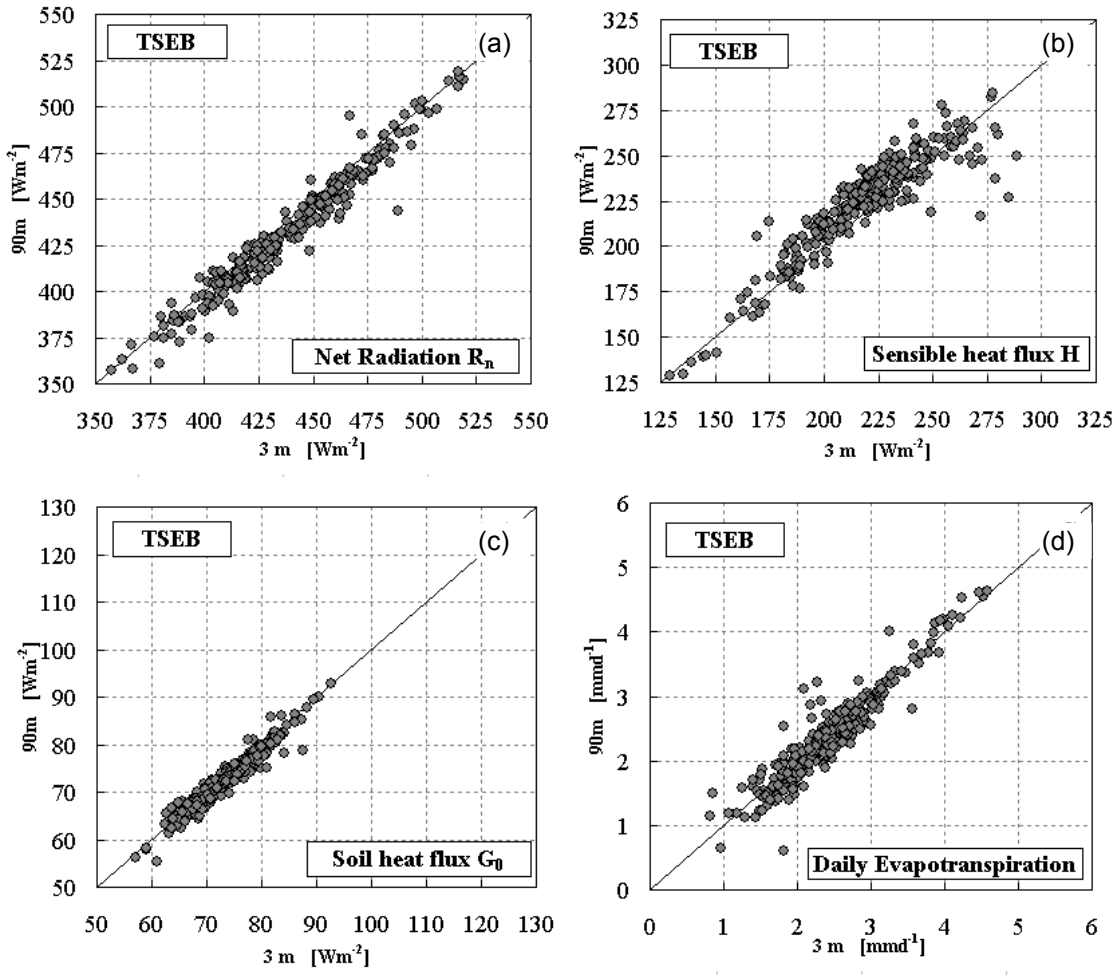

Fig. 6 Scatterplots of 3-m *vs* 90-m model outputs obtained using TSEB.

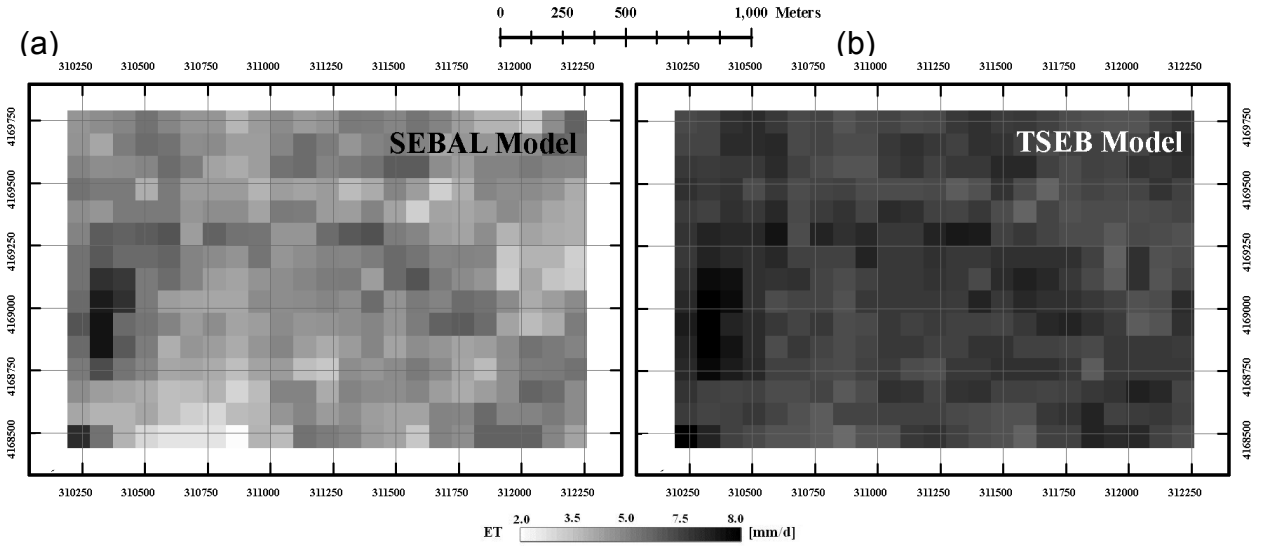

Fig. 7 Daily ET maps obtained from ASTER imagery using (a) SEBAL and (b) TSEB models.

obtained by using the higher pixel size resolution. This overestimation affects the ET_d values, which are underestimated by about 1 mm d^{-1}. The same effect has been not found when applying the TSEB model. It seems that TSEB is weakly affected by the pixel size degradation as shown in Fig. 6(a)–(d).

SEBAL *vs* TSEB: ASTER data

The effect of the pixel degradation has also been analysed by applying the SEBAL and TSEB models to ASTER data, with similar results as observed with the NERC degraded data set. Also in this case the tendency to underestimate the daily ET using SEBAL is confirmed comparing the two maps in Fig. 7(a),(b) and Fig. 8(a–c). The ET_d underestimates are mainly due to an overestimate of the sensible heat fluxes. These underestimates range between 50 and 90 W m^{-2}.

The G_0 values analysis confirms as observed for the NERC data analysis: the SEBAL model estimates an almost constant value for G_0 (about 90 W m^{-2}) while the TSEB G_0 estimations range between 70 and 120 W m^{-2}.

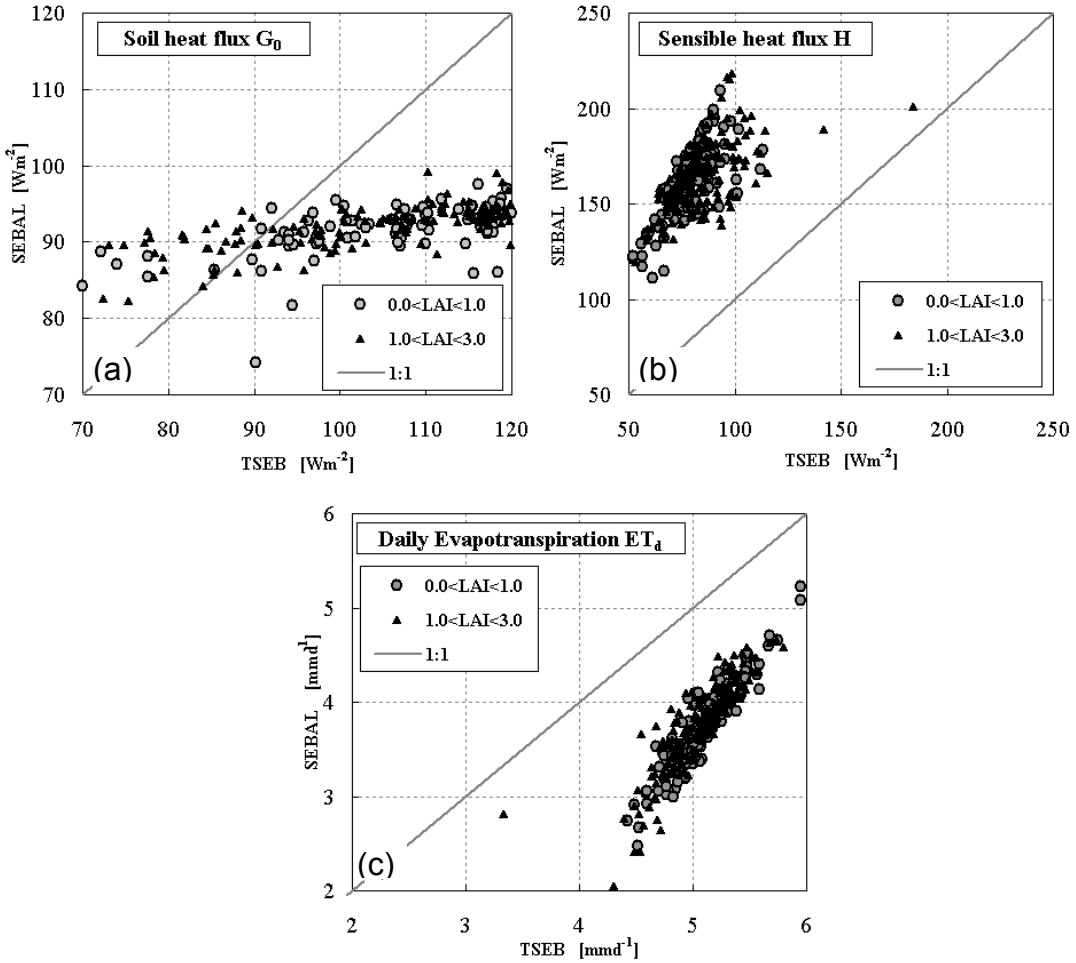

Fig. 8 Scatterplots of SEBAL *vs* TSEB modelled fluxes and evapotranspiration outputs derived using ASTER data set.

DISCUSSION AND CONCLUSIONS

The purpose of this work has been the comparison of two different energy balance models in the actual evapotranspiration estimation in a Mediterranean region. We focused the attention to the main conceptual differences between "single-layer" and "two-layer" approaches by the application of the well known SEBAL (Bastiaanssen *et al*., 1998a,b) and TSEB (Norman *et al.*, 1995) models. The comparison has been carried out using airborne multispectral imagery and a satellite ASTER image in order to investigate the pixel size effect on fluxes computation.

As a general conclusion we can confirm that the SEBAL model suffers a general overestimation of sensible heat fluxes H caused by the underestimation of the aerodynamic resistance to the heat transport which does not take into account the soil-canopy interaction.

For the aims of this study, focused to the evaluation of ET_d, this effect is compensated for by an overestimation of soil heat flux, especially for the high spatial resolution airborne images. This behaviour produces similar ET_d estimations compared to the TSEB ones.

The pixel size dimension is crucial for these applications, especially in Mediterranean semiarid regions where agriculture fields are typically of the order of hectares. From this point of view, the case study showed that the spatial resolution of the ASTER thermal band can be considered as an upper limit to correctly identify the spatial distribution of ET_d. However, applying the single layer model, the ASTER resolution seems to not be appropriate because the homogeneous land cover hypothesis is not respected. On the contrary the TSEB dual sources approach also gives reliable results in this case, because this model takes into account the soil–canopy interactions within the pixel.

To overtake this problem, an application of the disaggregation methods useful to obtain a better resolution synthetic thermal band using NDVI distribution, often available at finer pixel resolution, will be performed in the near future to improve ET_d estimations using coarser resolution (Kustas *et al*., 2003).

Acknowledgements This study has been carried out in the framework of the *"NERC Airborne Research & Survey Facility, 2005 Eastern Mediterranean Campaign"*. The authors are also grateful to Antonino Maltese for the airborne data geocorrection and to ENEA "Ente per le Nuove tecnologie, l'Energia e l'Ambiente", Italy, who provided the scintillometer measurements.

REFERENCES

Allen, R. G., Pereira, L. S., Raes, D. & Smith, M. (1998) *Crop evapotranspiration. Guidelines for computing crop water requirements*. FAO Irrigation and Drainage Paper (56), Rome, Italy.

Bastiaanssen, W. G. M. (1998) Remote sensing in water resources management: the state of the art. International Water Management Institute, Colombo, Sri Lanka.

Bastiaanssen, W. G. M., Menenti M., Feddes R. A. & Holtslag, A. A. M. (1998a) The Surface Energy Balance Algorithm for Land (SEBAL): Part 1 formulation. *J. Hydrol*. **212–213**, 198–212.

Bastiaanssen, W. G. M., Pelgrum, H., Wang, J., Ma, Y., Moreno, J., Roerink, G. J. & van der Wal, T. (1998b) The Surface Energy Balance Algorithm for Land (SEBAL): Part 2 validation. *J. Hydrol*. **212–213**, 213–229.

Brutsaert, W. (1982) *Evaporation into the Atmosphere. Theory, History and Applications*. D. Reidel Publ. Co., Dordrecht, The Netherlands.

Brutsaert, W. & Sugita, M. (1992) Regional surface fluxes from satellite-derived surface temperatures (AVHRR) and radiosonde profiles. *Bound. Layer Met*. **58**, 355–366.

Chavez, P. S. (1988) An improved dark-object subtraction technique for atmospheric scattering correction of multispectral data. *Remote Sens. Environ.* **24**, 459–479.

Chehbouni, A., Nichols, W. D., Njoku, E. G., Qi, J., Kerr, Y. & Cabot, F. (1997) A three component model to estimate sensible heat flux over sparse shrubs in Nevada. *Remote Sensing Rev.* **15**, 99–112.

Ciraolo, G., D'Urso, G. & Minacapilli, M. (2006) Actual evapotranspiration estimation by means of airborne and satellite remote sensing data. In: *Proc. Remote Sensing for Agriculture, Ecosystems and Hydrology VIII*. (ed. by M. Owe, G. D'Urso & C. Neale). SPIE Europe, Stoccolma, Italy.

Crago, R. D. (1996) Conservation and variability of the evaporative fraction during the daytime. *J. Hydrol*. **180**, 173–194.

Epema, G. F. (1990) Determination of planetary reflectance for Landsat 5 Thematic Mapper tapes processed by Earthnet. *Esa J.* **14**, 101–108.

Goudriaan, J. (1977) *Crop micrometeorology: a simulation study*. Center for Agric. Publ. and Doc., Wageningen, The Netherlands.

Kustas, W. P. & Norman, J. M. (1996) Use of remote sensing for evapotranspiration monitoring over land surfaces. *Hydrol. Sci. J.* **41**(4), 495–516.

Kustas, W. P. & Norman, J. M. (1999a) A two-source energy balance approach using directional radiometric temperature observations for sparse canopy covered surface. *Agronomy J.* **92**, 847–854.

Kustas, W. P. & Norman, J. M. (1999b) Evaluation of soil and vegetation heat flux predictions using a simple two-source model with radiometric temperature for partial canopy cover. *Agric. For. Met.* **94**, 13–29.

Kustas, W. P., Norman, J. M., Anderson, M. C. & French, A. N. (2003) Estimating subpixel surface temperatures and energy fluxes from the vegetation index-radiometric temperature relationship. *Remote Sens. Environ.* **85**, 429–440.

Menenti, M. (2000) Evaporation. In: *Remote Sensing in Hydrology and Water Management* (ed. by G. A. Schultz & E. T. Engman), 157–188. Springer Verlag, Berlin, Germany.

Menenti, M. & Choudhury, B. J. (1993) Parameterization of land surface evaporation by means of location dependent potential evaporation and surface temperature range. In: *Exchange Processes at the Land Surface for a Range of Space and Time Scales* (ed. by H. J. Bolle, R. A. Feddes & J. D. Kalma), 561–568. IAHS Publ. 212. IAHS Press, Wallingford, UK.

Norman, J. M., Kustas, W. P. & Humes, K. S. (1995) A two-source approach for estimating soil and vegetation energy fluxes in observations of directional radiometric surface temperature. *Agric. For. Met*. **77**, 263–293.

Priestley, C. H. B. & Taylor, R. J. (1972) On the assessment of surface heat flux and evaporation using large-scale parameters. *Mon. Weath. Rev.* **100**, 81–92.

Savige, C., Western, A., Walker, J. P., Kalma, J. D., French, A. & Abuzar, M. (2005) Obtaining surface energy fluxes from remotely sensed data. In: *Proc. Modelling and Simulation* (ed. by A. Zerger & R. M. Argent), 2946–2952, MODSIM 2005 Society of Australia and New Zealand.

Schumugge, T. J., Kustas W. P., Ritchie J. C., Jackson T. J. & Rango, A.. (2002) Remote sensing in hydrology. *Adv. Water Resour*. **25**, 1367–1385.

Slater, P., Biggar, S., Thome, K., Gellman, D. & Spyak, P. (1996) Vicarious radiometric calibrations of EOS sensors. *J. Atmos. Ocean Technol.* **13**, 349–359.